Acta Geochim
https://doi.org/10.1007/s11631-019-00338-w

ORIGINAL ARTICLE

Metallogenic controls on the granite-related W–Sn deposits in the Hunan–Jiangxi region, China: evidence from zircon trace element geochemistry

Yuannan Feng[1,2] · Tingguang Lan[1] · Lichuan Pan[1] · Tingting Liu[3] · Shaohua Dong[1]

Received: 13 September 2018 / Revised: 12 March 2019 / Accepted: 29 March 2019

Abstract The Nanling Range in South China is well known for its rich granite-related W–Sn deposits. To elucidate the controls of different granite-related W–Sn metallogenesis in the region, we chose five representative ore-related granites (Yanbei, Mikengshan, Tieshanlong, Qianlishan, and Yaogangxian intrusions) in the Hunan–Jiangxi region, and studied their magmatic zircon ages and trace element geochemistry. Our new zircon data showed the differences in ages, temperatures and oxygen fugacity of the ore-forming magmas. Zircon U–Pb ages of the Yanbei and Mikengshan intrusions are characterized by 142.4 ± 2.4 and 143.0 ± 2.3 Ma, respectively, whereas the Tieshanlong and Qianlishan intrusions are 159.5 ± 2.3 and 153.2 ± 3.3 Ma, respectively. The Sn-related intrusions were younger than the W-related intrusions. The Ti-in-zircon thermometry showed that there was no systematic difference between the Sn-related Yanbei (680–744 °C) and Mikengshan (697–763 °C) intrusions and the W-related Tieshanlong (730–800 °C), Qianlishan (690–755 °C) and Yaogangxian (686–751 °C) intrusions. However, the zircon Ce^{4+}/Ce^{3+} ratios of the Yanbei (averaged at 18.3) and Mikengshan (averaged at 18.8) intrusions are lower than those of the Tieshanlong (averaged at 36.9), Qianlishan (averaged at 38.4) and Yaogangxian (averaged at 37) intrusions, indicating that the Sn-related granitic magmas might have lower oxygen fugacities than those of the W-related. This can be explained by that, in more reduced magmas, Sn is more soluble than W and thus is more enriched in the residual melt to form Sn mineralization. The difference in source materials between the Sn-related and the W-related granites seems to have contributed to the different redox conditions of the melts.

Keywords W–Sn deposits · South China · Zircon trace element chemistry · Ti-in-zircon thermometry · Oxygen fugacity

1 Introduction

Physicochemical conditions of magmas, such as temperature, pressure, oxygen fugacity, and water content, impose key controls on the ore fertility and on what types of ore deposits are to be formed (Richards 2011, 2013). Since ore-forming intrusions are commonly altered, conventional whole-rock geochemistry cannot precisely constrain the nature of the ore-forming magmas. In recent years, with the rapid development of LA-ICP-MS technology, in situ mineral geochemical analyses have been widely used to determine the physicochemical features of the magmas. Zircon ($ZrSiO_4$) is a common accessory mineral in many types of rocks, and an important carrier for REEs (rare earth elements), HFSEs (high field strength elements). It's also physiochemically inert and contains high U and Th contents and very low common Pb contents (Watson et al. 1997), making it an ideal candidate for U–Pb dating. The

Electronic supplementary material The online version of this article (https://doi.org/10.1007/s11631-019-00338-w) contains supplementary material, which is available to authorized users.

✉ Tingguang Lan
lantingguang@126.com

[1] State Key Laboratory of Ore Deposit Geochemistry, Institute of Geochemistry, Chinese Academy of Sciences, Guiyang 550081, China

[2] University of Chinese Academy of Sciences, Beijing 100049, China

[3] The Fifth Geology Company of Hebei Geology and Mineral Bureau, Tangshan 063000, China

Published online: 08 April 2019

low solubility, high melting point and physical resistivity of zircon (Hoskin and Schaltegger 2003; El-Bialy and Ali 2013) enable it to retain the original trace element chemistry (except for radiogenic elements, e.g., U and Th). During the zircon crystallization, a specific suite of trace elements (e.g., Sc, Y, Ti, Hf, Th, U, Nb, Ta, V, P and REEs) is incorporated into the crystal lattice, and the variation of their concentrations indicates their geological formation processes (El-Bialy and Ali 2013). Currently, zircon trace element geochemistry were widely used to study the compositions (e.g., Heaman et al. 1990; Belousova et al. 2002; Hanchar and van Westrenen 2007), oxidation states (e.g., Ballard et al. 2002; Trail et al. 2012; Burnham and Berry 2014; Smythe and Brenan 2016) and crystallization temperatures (e.g., Watson and Harrison 2005; Watson et al. 2006; Ferry and Watson 2007) of the host magmas. Therefore, zircon is regarded as an effective petrogenetic/metallogenic indicator.

The Nanling Range in South China is a world-class W–Sn province, and hosts a large number of Yanshanian (Jurassic-Cretaceous) granitoids and associated W–Sn deposits (Hua et al. 2003; Chen et al. 2008, 2013; Li et al. 2007; Hu and Zhou 2012; Wei et al. 2012; Hu et al. 2012a, b, 2015, 2017a, b; Mao et al. 2013). Previous studies in this region were dedicated mainly to the petrography, geochronology and petrogenesis of the ore-forming granitoids, whereas the critical factors controlling the W and Sn mineralization were poorly understood. Therefore, in this study, we select representative intrusions associated with W and Sn mineralization from the Nanling Range (e.g., the W-related Tieshanlong, Qianlishan and Yaogangxian granites and the Sn-related Yanbei and Mikengshan granites) to conduct whole-rock major and trace element analyses and LA-ICP-MS zircon U–Pb dating and trace element analyses, with the aim to discuss the physiochemical difference (mainly temperature and oxygen fugacity) between the W-related and Sn-related granitoids. Our studies intend to elucidate the critical factors controlling the W and Sn mineralization associated with the granitoids.

2 Regional geology

In this study, we focused on the famous W–Sn associated granitoids in southern Jiangxi (Huangsha W, Yanbei Sn and Taoxiba Sn deposits) and southern Hunan (Shizhuyuan W-polymetallic and Yaogangxian W deposits) areas in the Nanling Range (Fig. 1). The southern Jiangxi region is where the W deposits are most concentrated. Igneous rocks (ca. 600–66 Ma) are widely distributed in this region, among which granitic rocks (180–66 Ma) are the most pervasive, and include mainly biotite granite, granite porphyry and granodiorite complexes. The southern Hunan W–Sn polymetallic ore district contains a large number of diachronous and multiphase intermediate-felsic granitoids, whose distributions are controlled by the boundary between the uplift zone (ca. 600–400 Ma) and depression (409–205 Ma), as well as by the basement architecture and regional-scale deep faults. The granitoid belts in the region are mostly NE-trending and minor NW-trending (Wang 2008).

The Huangsha W deposit is located in the intersection between the E-W-trending Dayu-Ruijin fold belt and the NE-NNE-trending Yushan fold belt (Gan 1988), and is a large-scale, polymetallic sulfide-bearing quartz-vein-type W deposit in southern Jiangxi. Major strata exposed in the mine include the Cambrian, Devonian and Quaternary sequences, and multi-phase magmatic intrusions were documented (Li 2011). The Tieshanlong granite is metallogenically related to the Huangsha W deposit, and is located in the central part of Huangsha. The intrusion comprises medium-to coarse-grained porphyritic biotite granite. Rock-forming minerals mainly include quartz, plagioclase, muscovite and biotite, with accessory minerals of zircon and sphene (Li 2011). Huang et al. (2011) reported SHRIMP zircon U–Pb age of 168.1 ± 2.1 Ma for the Tieshanlong biotite granite. The Tieshanlong intrusive complex has very low $\varepsilon_{Nd}(t)$ values (− 15.5 to 11.8), indicating that the magmas were probably sourced from the Paleoproterozoic crustal basement (Li 2011).

The super-large Yanbei porphyry Sn deposit is located in the west of the intersection between the N-trending Shicheng-Xunwu fault and the Huichang ring-shaped structure, belonging to the southern Wuyi Mountains REM (rare earth metals)-W–Sn metallogenic belt. The deposit is hosted in the late Jurassic Huichang intermediate-felsic volcanic basin, and the orebodies are clustered along the contact between the granite porphyry and rhyolite porphyry (Mei et al. 2007). The ore-related porphyritic granite of the Yanbei Sn deposit is grey and massive, and contains mainly quartz and K-feldspar and minor biotite. Accessory minerals include zircon, pyrite, chalcopyrite and cassiterite. The ore-related intrusion shows zircon U–Pb age of 137.4 ± 1.2 Ma. This intrusion has relatively high $\varepsilon_{Nd}(t)$ values (− 9.9 to − 10.1), which fall into the fields of the Proterozoic Longquan and Mayuan groups crustal rocks (Liang 2017).

The Taoxiba Sn deposit (Huichang County, Jiangxi) is located in the northern part of the Mikengshan intrusion in the Xikengjing ore field, about 3 km away from the Yanbei Sn deposit. Tectonically, the Taoxiba deposit is situated in the intersection between the western margin of the Mesozoic volcanic-metallogenic belt of the SE China coast and the EW-trending South China Sn belt. The two belts collided with each other at ~ 400 Ma (Li 2011). The ore-

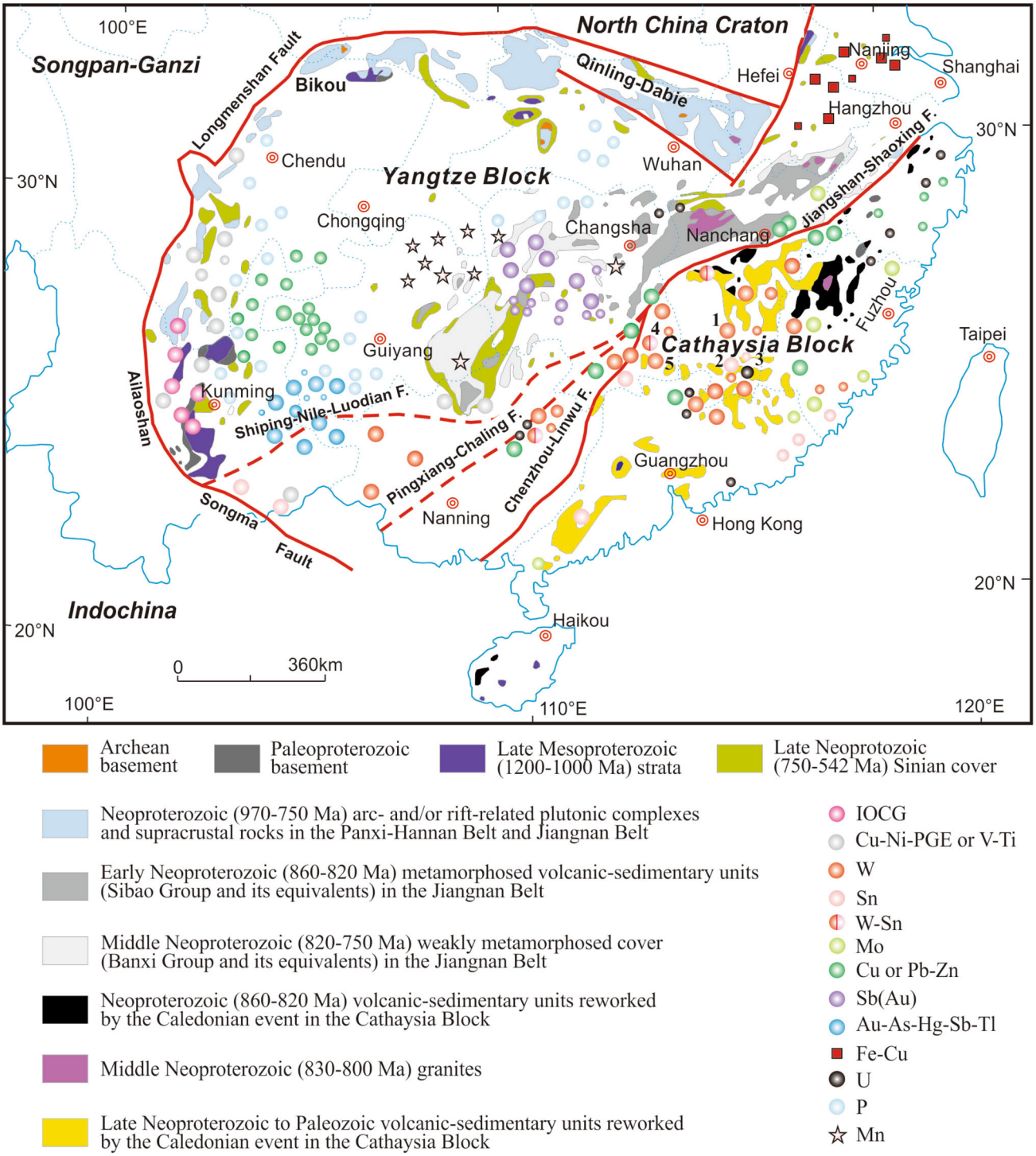

Fig. 1 Simplified geological map showing the structural framework of the South China and the distribution of ore deposits (Ore deposits in this study include: 1-Huangsha W deposit, 2-Yanbei Sn deposit, 3-Taoxiba Sn deposit, 4- Shizhuyuan W polymetallic deposit and 5-Yaogangxian W deposit) (modified after Mao et al. 2011; Hu et al. 2017a)

related Mikengshan intrusive complex comprises mainly porphyritic biotite (K-feldspar) granite. The intrusion shows the zircon U–Pb age of 136.0 ± 1.7 Ma (Qiu et al. 2006), and has relatively high $\varepsilon_{Nd}(t)$ values (− 3.6 to − 5.1), which might be derived from a crust-mantle mixed source (Qiu et al. 2005).

The Shizhuyuan W-polymetallic deposit is located at the eastern margin of the Hercynian-Indosinian depression of the South China Caledonian fold belt (Chen 1993). The

ore-related Qianlishan granites (southeast of Chenzhou City, Hunan) are located in the middle part of the Nanling metallogenic belt, and may have formed in three phases: (I) porphyritic biotite granite (158–157 Ma), (II) equigranular biotite granite (158–155 Ma) and (III) granite porphyry (~ 154 Ma) (Wu et al. 2011; Chen et al. 2016). The various intrusive phases of the Qianlishan granites have overlapping ranges of initial Sr isotopic compositions. In the ε_{Nd} versus ε_{Sr} diagram, almost all the plots fall on a horizontal line, consistent with the Yangtze continental crust-derived granite. This suggests that the Qianlishan granites were mainly sourced from the re-melting of crustal materials (Shen et al. 1995).

The Yaogangxian deposit in Hunan province is an important W deposit in the Nanling Range. The deposit and its host Yaogangxian granitic complex are located in the northern part of the Nanling tectonic belt (Peng et al. 2006; Hu et al. 2012b). Zircon U–Pb ages of the medium- to coarse-grained two-mica granite, fine- to medium-grained two-mica granite and fine-grained muscovite granite are 169.5 ± 0.9 and 170.7 ± 1.5 Ma, 161.6 ± 0.7 and 162.6 ± 0.6 Ma, 156.9 ± 0.7 and 157.1 ± 0.7 Ma, respectively (Dong 2012). The coarse-grained two-mica granite is light grey, massive and porphyritic, and mainly contains quartz, K-feldspar and plagioclase with minor biotite and muscovite. Accessory minerals include apatite, garnet, zircon and xenotime (Dong 2012). The medium- to fine-grained two-mica granite comprises mainly quartz, K-feldspar, plagioclase, muscovite and biotite, with accessory minerals including apatite, garnet, zircon, xenotime and fluorite (Dong 2012). The fine-grained muscovite granite comprises mainly quartz, K-feldspar, plagioclase and muscovite, with accessory minerals of garnet, zircon and fluorite (Dong 2012). Published whole-rock geochemical and Sr–Nd isotopic data suggest that the Yaogangxian granitic magmas were mainly sourced from Paleoproterozoic argillaceous rocks (Dong 2012).

3 Analytical methods

Whole-rock major and trace element analyses were conducted at the ASL Laboratory in Guangdong province. For major element analyses, $Li_2B_4O_7$ powders were admixed with 200 mesh whole-rock powders and then fused into glass discs. After that, a Philips PW2404 XRF analyzed the discs. Using basaltic to granitic rock standards (NCSDC73303, SARM-2, SARM-3, and SARM-4) to monitor the analytical quality, and the results indicate the accuracy better than 2%. For trace element analyses, whole-rock powders were dissolved in distilled $HF + HNO_3 + HClO_4$ mixture, dried, and then digested with HCl. An Agilent 7700×ICP-MS analyzed the final solutions. The analytical uncertainties are within 5% for most elements, as indicated by the analytical results of the standard materials (GBM908-10, MRGeo08, OREAS460 and SY-4).

Zircon U–Pb dating and trace element analyses were performed at the State Key Laboratory of Ore Deposit Geochemistry, Institute of Geochemistry, Chinese Academy of Sciences, using a Geolas Pro 193 nm laser ablation system coupled with an Agilent 7900 ICP-MS. Analytical conditions were 32 μm laser beam and 6 Hz frequency. Zircon 91500 was used as an external standard, and elemental content calibration was performed using NIST SRM610 as an external standard and Zr as an internal standard. Details of the analytical processes were described in Liu et al. (2008, 2010a, b).

4 Results and discussion

4.1 Zircon U–Pb dating

Zircon U–Pb data are listed in Table S1, and the Concordia diagrams are shown in Fig. 2.

All the analyzed spots of the Qianlishan intrusion (sample CS007; Shizhuyuan W-polymetallic deposit), Tieshanlong intrusion (sample TSL02; Huangsha W deposit), Yanbei intrusion (sample YB01; Yanbei Sn deposit) and Mikengshan intrusion (sample LHS02; Taoxiba Sn deposit) fall on the Concordia, with their weighted mean $^{206}Pb/^{238}U$ ages of 153.2 ± 3.3 (MSWD = 3.2, n = 20), 159.5 ± 2.3 (MSWD = 2, n = 22), 142.4 ± 2.4 (MSWD = 2.6, n = 24) and 143 ± 2.3 Ma (MSWD = 2, n = 20), respectively. These zircon U–Pb ages indicate that the Sn-related granitoids (~ 140 Ma) formed much later than the W-related ones (> 150 Ma) in this study, suggesting that the magmas related to the Sn and W mineralization were probably derived from two independent magmatic events (Figs. 3, 4).

4.2 Whole-rock major and trace elements

For major element compositions, all the studied intrusions are calc-alkaline (Rittmann index: 1.87–2.61), metaluminous to weakly peraluminous (A/CNK = 1.00–1.24). Compared with the other four intrusions, the Qianlishan granite is more felsic. In the primitive-mantle normalized spider diagram, all the five intrusions show obvious Ba, Sr, P and Ti depletions. The chondrite-normalized REE patterns of Yaogangxian show a weak tetrad effect, while those of the other four intrusions incline to right. The Yanbei intrusion contains the highest average ∑REE contents (380 ppm) and La_N/Yb_N ratios (11.6). The

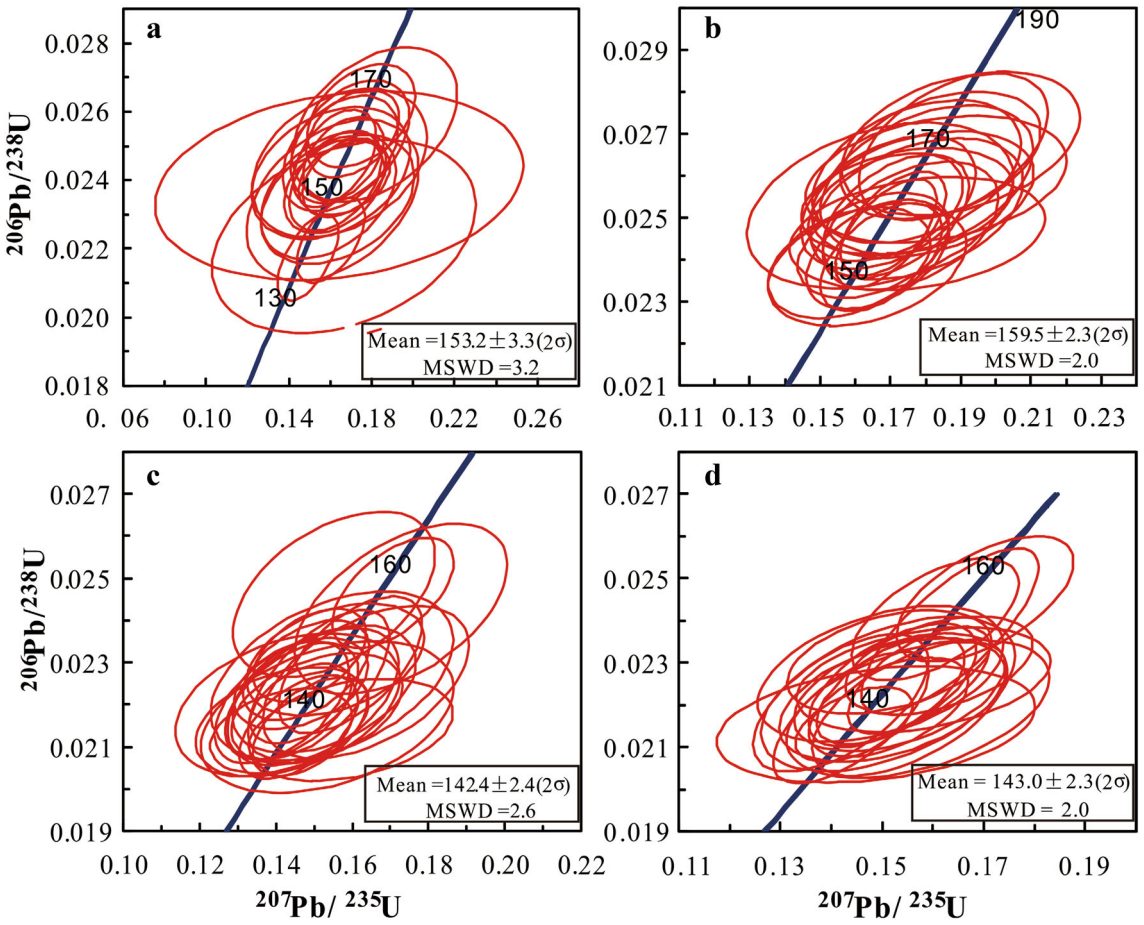

Fig. 2 Zircon U–Pb Concordia diagrams of Qianlishan porphyritic biotite granite (**a**), Tieshanlong medium- to fine-grained porphyritic biotite granite (**b**), Yanbei porphyritic K-feldspar granite (**c**) and Mikengshan coarse-grained biotite granite (**d**)

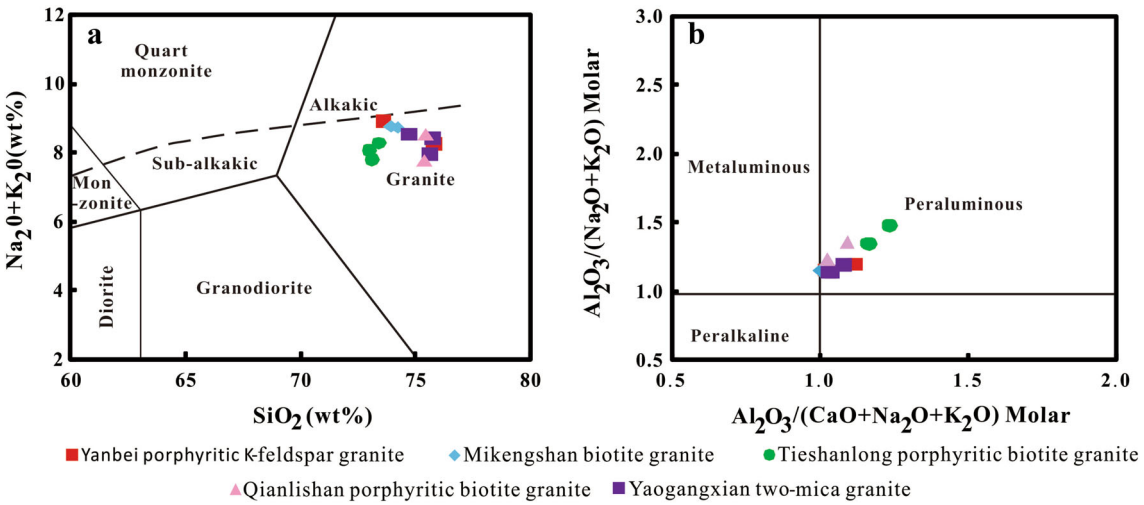

Fig. 3 Plots of $Na_2O + K_2O$ (wt%) versus SiO_2 (wt%) (**a**) and $Al_2O_3/(Na_2O + K_2O)$ molar versus $Al_2O_3/(CaO + Na_2O + K_2O)$ molar (**b**)

Mikengshan, Tieshanlong and Qianlishan intrusions show medium ∑REE and La_N/Yb_N, while the Yaogangxian intrusion shows the lowest average ∑REE (66.3 ppm), La_N/Yb_N (0.43) and strongest Ce anomaly (1.28) (Table 1).

4.3 Zircon geochemistry

The zircon Th/U ratios are all > 0.1 (mostly > 0.4), indicating typical magmatic zircons (Belousova et al. 2002;

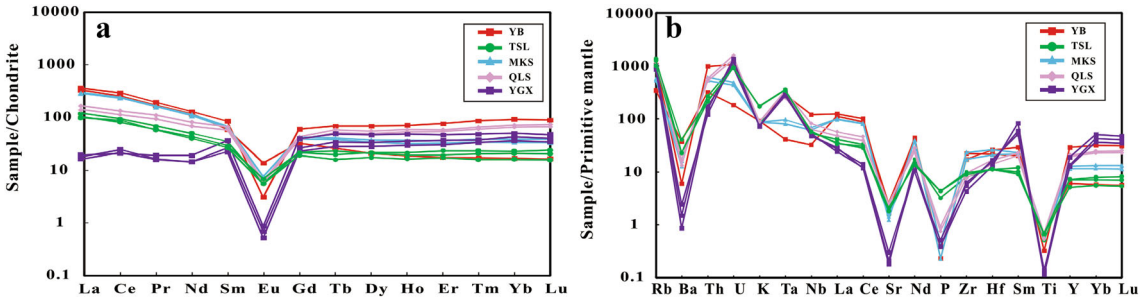

Fig. 4 Whole-rock chondrite-normalized REE distribution patterns (**a**) and primitive-mantle normalized spider diagram (**b**) (normalization values after Sun and McDonough 1989)

Wu and Zheng 2004) (CL images in Fig. 5). The zircons in the Mikengshan intrusion contain distinctly higher REE, Th, U, Ta, Nb, Ce and Zr contents than those in the other four intrusions. The zircons in the Yanbei intrusion contain the lowest zircon Ti contents. All the intrusions show very similar zircon REE distribution patterns, as featured by LREE depletion, HREE enrichment and distinct positive Ce and negative Eu anomalies. Among the five intrusions, the zircons in the Mikengshan intrusion have the highest $\sum$REE and La_N/Yb_N, while the Tieshanlong and Yaogangxian intrusions have the highest positive Ce anomalies and the highest negative Eu anomalies, respectively (Tables 2 and S2).

Ce anomaly in zircon is calculated from $\left(\frac{Ce}{Ce^*}\right)_D = \frac{D_{Ce}^{zrc/melt}}{\sqrt{D_{La}^{zrc/melt} \times D_{Pr}^{zrc/melt}}}$ (Trail et al. 2011, 2012), where $D_{Ce}^{zrc/melt}$, $D_{La}^{zrc/melt}$ and $D_{Pr}^{zrc/melt}$ represent the concentrations of Ce, La, and Pr in zircon to that of the melt, respectively. Eu anomaly in zircon is calculated from $\left(\frac{Eu}{Eu^*}\right)_D = \frac{D_{Eu}^{zrc/melt}}{\sqrt{D_{Sm}^{zrc/melt} \times D_{Gd}^{zrc/melt}}}$ (Trail et al. 2011, 2012), where $D_{Eu}^{zrc/melt}$, $D_{Sm}^{zrc/melt}$, and $D_{Gd}^{zrc/melt}$ represent the concentrations of Eu, Sm, and Gd in zircon to that of the melt, respectively.

4.4 Ti-in-zircon temperatures

Numerous studies have shown that Ti-in-zircon thermometry can effectively constrain the crystallization temperatures of zircons (Watson and Harrison 2005; Watson et al. 2006; Ferry and Watson 2007). The Ti-in-zircon thermometer (Ferry and Watson 2007) is commonly given as,

$$T = \frac{(4800 \pm 86)}{(5.711 \pm 0.072) - \log(\mathrm{Ti}) - \log a_{SiO_2} + \log a_{TiO_2}} - 273.15. \quad (1)$$

The Yaogangxian and Yanbei intrusions contain accessory mineral of rutile (Li et al. 2007; Wang et al. 2014), thus the α_{TiO2} can be set to 1. The estimation of α_{TiO2} in the Tieshanlong, Qianlishan, Mikengshan granites was based on the method of Hayden and Watson (2007), which shows that $\log Ti_{melt}(ppm) = 7.95–5305/T(K) + 0.124FM$ (FM = 1/Si × (Na + K+2(Ca + Mg + Fe))/Al (cation fractions). According to this method, only 582–592 ppm Ti could lead to the rutile saturation in the Tieshanlong, Qianlishan, Mikengshan granites. The above granites contain 659–905 ppm Ti, suggesting TiO_2 saturation in their melts. In addition, all the granites contain quartz grains. Therefore, the αSiO_2 and αTiO_2 of all the granites can be set to 1, the above equation can be simplified into:

$$T = \frac{(4800 \pm 86)}{(5.711 \pm 0.072) - \log(\mathrm{Ti})} - 273.15 \quad (2)$$

According to Eq. (2), the calculated temperatures for the Mikengshan, Yanbei, Tieshanlong, Qianlishan and Yaogangxian granites are 697–763, 680–744, 730–800, 690–755, 686–751 °C, respectively. The results show that there is no systematic difference in zircon crystallization temperatures between the W- and Sn-related granites (Figs. 6, 7).

4.5 Zircon Ce^{4+}/Ce^{3+} indicator on magma oxygen fugacity

Ce anomaly in zircon can reflect the physicochemical conditions of zircon crystallization (Ballard et al. 2002; Pettke et al. 2005; Barth and Wooden 2010; Claiborne et al. 2010; Trail et al. 2011, 2012; Burnham and Berry 2012; Li et al. 2012). Previous studies suggested that zircon Ce^{3+} and Ce^{4+} are strongly fractionated with magma redox changes, but unaffected by the fractionation of minerals. This suggests that Ce^{4+}/Ce^{3+} ratios can effectively reflect the relative oxygen fugacity of magma (Ballard et al. 2002). The zircon Ce^{3+} and Ce^{4+} can be calculated using the method of Ballard et al. (2002):

Table 1 Major (wt%) and trace (ppm) elements of the Yanbei, Tieshanlong, Mikengshan, Yaogangxian and Qianlishan granites

Sample	Yanbei		Tieshanlong			Mikengshan		Yaogangxian			Qianlishan	
	Porphyritic K-feldspar graniteand		Porphyritic biotite granite	Porphyritic biotite granite (Li 2011)	Granite porphyry (Li 2011)	Biotite granite		Two-mica granite (Dong 2012)			Porphyritic biotite granite	
	16YB-01	16YB-05	16TSL-02	TS24	TS-8	16LHS-01	16LHS-02	YGX-19-2	YGX-19-12	YGX-23-21	CS007-1	CS007-7
SiO_2 (wt%)	73.6	75.8	73	14.4	14.4	74.2	74	75.7	75.8	74.7	75.5	75.4
Al_2O_3	13.7	12.2	13.9	0.38	0.29	13.0	12.9	12.5	12.9	13	13.5	13.1
Na_2O	3.39	3.11	3.18	3.16	2.60	3.55	3.5	3.6	4.09	4.13	3.31	2.43
K_2O	5.54	5.16	4.89	5.16	5.20	5.21	5.29	4.39	4.36	4.43	5.26	5.35
CaO	0.40	0.72	0.77	0.88	0.94	0.80	0.81	0.52	0.61	0.53	1.12	1.21
TiO_2	0.15	0.07	0.11	0.13	0.13	0.13	0.15	0.03	0.03	0.03	0.15	0.12
TFe_2O_3	2.11	1.4	1.57	1.41	1.52	2.06	2.1	1.09	0.86	0.98	1.16	1.07
MgO	0.16	0.05	0.27	0.22	0.44	0.08	0.11	0.01	0.02	0.04	0.14	0.25
MnO	0.05	0.03	0.12	0.11	0.15	0.04	0.04	0.14	0.14	0.13	0.03	0.03
P_2O_5	0.02	0.01	0.14	0.19	0.19	0.01	0.02	0.01	0.01	0.01	0.04	0.03
A/CNK	1.11	1.02	1.17	1.16	1.24	1.01	1.00	1.08	1.03	1.04	1.02	1.09
Rb (ppm)	220	666	853	643	796	338	360	639	539	597	779	730
Ba	263	42.2	157	158	282	89.8	116	10.3	5.99	16.8	92.5	117
Th	27.0	83.2	22.3	17.9	18.1	51.8	45.2	14.5	12.7	10.2	48.7	43.7
U	3.86	22.3	21.1	19.6	19.3	10.2	9.22	19.6	28.3	25.4	33.0	27.4
Ta	1.70	11.6	11.5	14.1	14.6	3.30	4.00	12.6	11.2	11.6	13.8	10.3
Nb	23.1	86.1	38.1	41.4	40.0	43.5	48.8	33.9	37.8	34.1	58.2	44.7
Sr	54.4	35.2	32.5	44.1	38.0	26.4	30.3	3.78	4.43	6.25	48	53.1
P	43.6	21.8	305	415	415	21.8	43.6	36.2	37.1	48	86.6	71.4
Zr	251	193	89	100	109	194	264	48	70.1	61.6	107	85.6
Hf	6.70	8.00	3.50	3.49	3.46	6.50	8.10	3.99	4.85	5.15	5.21	4.31
Ti	899	420	659	853	886	779	899	162	150	180	905	701
Y	28.2	132	32.8	23.5	33.4	52.7	58.7	85.5	61.4	57.8	95	89
La	77.8	85.1	28.3	23.2	24.2	66.9	69.3	4.67	3.95	4.41	39	33
Ce	156	179	58.1	54.1	49.9	144	147	12.9	13.4	15.1	81.7	69.4
Pr	16.1	18.4	6.56	5.47	5.65	15.0	15.6	1.83	1.52	1.56	10.5	8.90
Nd	54.6	59.6	23.3	18.5	20.0	50.0	53.2	8.91	6.83	6.8	38.2	32
Sm	9.03	13.0	5.35	4.09	4.48	9.80	10.4	5.58	4.02	3.44	10.2	8.93
Eu	0.80	0.18	0.33	0.32	0.40	0.36	0.44	0.05	0.04	0.03	0.36	0.34
Gd	6.72	12.3	4.53	3.92	4.43	7.93	8.75	8.16	5.45	4.71	8.82	7.84
Tb	0.99	2.59	0.87	0.60	0.74	1.43	1.53	1.83	1.28	1.06	2.20	1.94
Dy	5.33	17.6	5.33	4.44	5.49	8.71	9.59	11.9	8.6	7.14	14.1	12.7
Ho	1.06	4.03	1.10	0.93	1.23	1.82	2.08	2.75	2.01	1.68	3.34	3.02
Er	2.92	12.7	3.22	2.87	3.87	5.42	5.95	7.79	6.11	5.05	9.70	8.96
Tm	0.44	2.22	0.53	0.41	0.60	0.88	0.99	1.24	0.96	0.86	1.66	1.55
Yb	2.87	15.8	3.55	2.75	3.93	5.78	6.66	8.55	7.29	6.18	12.2	11.2
Lu	0.42	2.29	0.52	0.40	0.61	0.85	0.99	1.2	1.03	0.88	1.86	1.7
Σ REE (ppm)	335	424	142	122	126	318	332	77.4	58.9	62.5	234	201
La_N/Yb_N	19.4	3.88	5.72	6.05	4.42	8.30	7.46	0.39	0.51	0.39	2.30	2.12
Ce anomaly	1.08	1.11	1.05	1.18	1.05	1.11	1.10	1.08	1.41	1.34	0.99	0.99
Eu anomaly	0.31	0.04	0.20	0.24	0.27	0.12	0.14	0.02	0.02	0.03	0.12	0.13

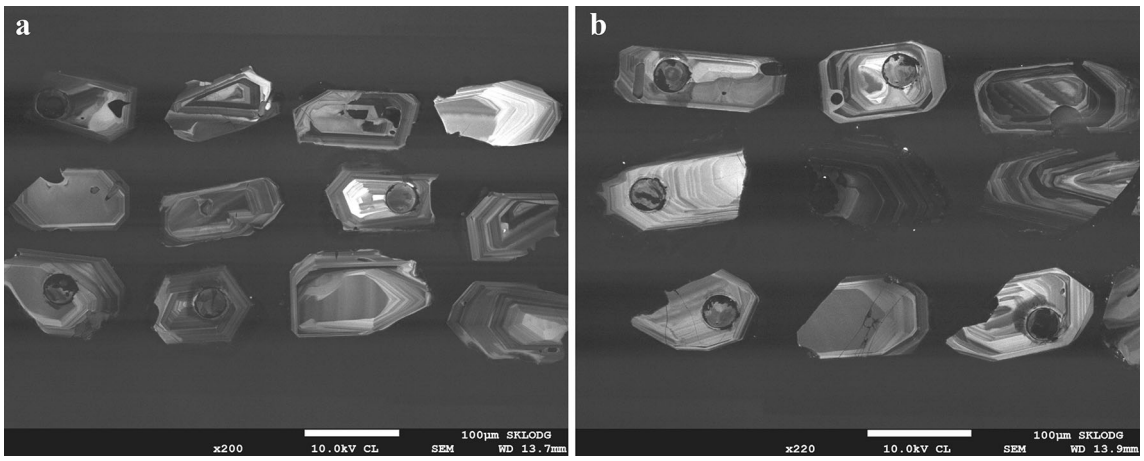

Fig. 5 CL images of zircons from **a** Yanbeiand, **b** Tieshanlong granites

Table 2 Zircon ∑REE, La_N/Yb_N, Ce and Eu anomalies for the five intrusions

Intrusion	Mineralization type	∑REE (ppm)	(La/Yb)N	Ce anomaly	Eu anomaly
Yanbei	Sn	1120	0.0048	61.4	0.94
Mikengshan	Sn	1343	0.0117	51.8	0.54
Tieshanlong	W	885	0.0004	71.4	0.70
Qianlishan	W-polymetallic	1230	0.0098	39.7	0.91
Yaogangxian	W	1222	0.0002	68.7	6.82

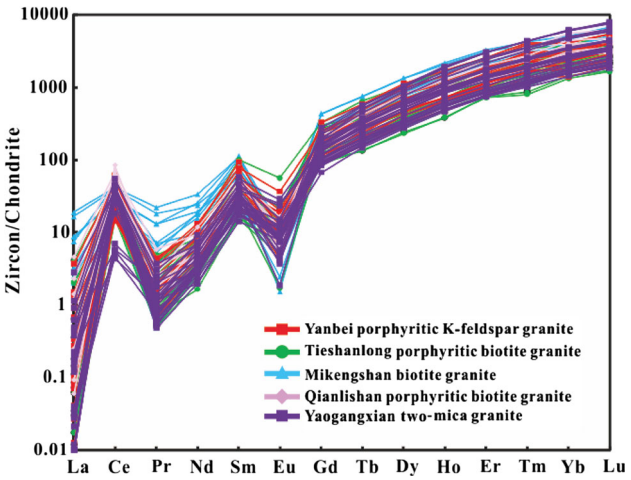

Fig. 6 Chondrite-normalized zircon REE distribution patterns of the five intrusions studied (normalization values after Sun and McDonough 1989)

$$(Ce(\mathrm{IV})/Ce(\mathrm{III}))_{zircon} = \frac{Ce_{melt} - \frac{Ce_{zircon}}{D^{zircon/melt}_{Ce(\mathrm{III})}}}{\frac{Ce_{zircon}}{D^{zircon/melt}_{Ce(\mathrm{IV})}} - Ce_{melt}} \quad (3)$$

In this equation, Ce_{zircon} and Ce_{melt} represent the Ce concentrations in zircon and melt, respectively. $D^{zircon/melt}_{Ce(III)}$ and $D^{zircon/melt}_{Ce(\mathrm{IV})}$ represent the zircon/melt partition coefficients of Ce^{3+} and Ce^{4+}, and they can be calculated based on the lattice-strain model (Ballard et al. 2002). As a result, the Sn-related Yanbei (averaged at 18.3) and Mikengshan (averaged at 18.8) intrusions show much lower Ce^{4+}/Ce^{3+} ratios than those of the W-related Tieshanlong (averaged at 37.0), Qianlishan (averaged at 38.4) and Yaogangxian (averaged at 37.0) intrusions (Table 3). This indicates that the W-related magmas might be more oxidized than the Sn-related magmas.

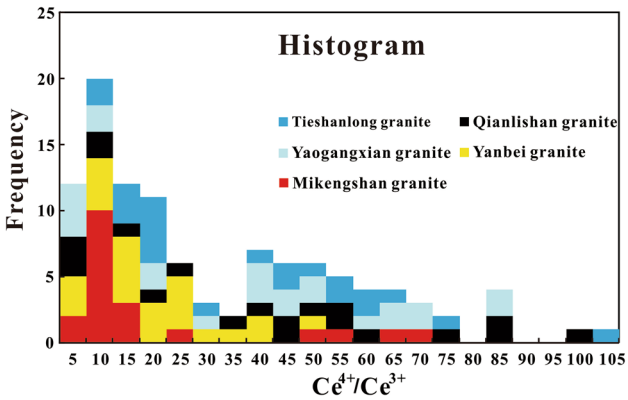

Fig. 7 Histogram of zircon Ce^{4+}/Ce^{3+} ratio versus frequency

Experiments have shown that the solubility of W is higher than that of Sn in more oxidized melts, while Sn is more soluble in more reduced melts (Blevin et al. 1996;

Table 3 Zircon Ce^{4+}/Ce^{3+} of the five intrusions

Intrusion	Mineralization type	$D^{zircon/melt}_{Ce(III)}$	$D^{zircon/melt}_{Ce(IV)}$	Ce_{melt} (ppm)	Ce_{zircon} (ppm)	$(Ce^{4+}/Ce^{3+})_{zircon}$
Yanbei	Sn	0.02	160	167	25.4	18.3
Mikengshan	Sn	0.02	220	145	32.7	18.8
Tieshanlong	W	0.01	223	58.1	14.0	37.0
Qianlishan	W-polymetallic	0.07	245	75.5	43.3	38.4
Yaogangxian	W	0.05	270	13.8	19.1	37.0

Linnen et al. 1996; Bhalla et al. 2005; Champion and Bultitude 2013; Che et al. 2013). The different oxygen fugacities of the W-related and Sn-related granites thus might have originally facilitated the W and Sn to be enriched in the more oxidized and more reduced magmas, respectively. Furthermore, the accessory minerals in the W-related Yaogangxian, Qianlishan, Tieshanlong are mainly magnetite, ilmenite, and sphene (Li 2011a; Tong 2013; Wang et al. 2014), whereas in the Sn-related Yanbei and Mikengshan granites are magnetite, cassiterite, topaz, fluorite and monazite (Yu et al. 2013; Li et al. 2007; Liang 2017). This indicates that Ti-bearing minerals are enriched in the W-related granites while F-bearing minerals are enriched in the Sn-related granites. At higher oxygen fugacity, Sn is presented dominantly as Sn^{4+} species (SnO_2) (Linnen et al. 1996). Because Sn^{4+} and Ti^{4+} species have similar ionic radii, Sn^{4+} will replace Ti^{4+} to enter the Ti-bearing minerals. Fractional crystallization of the Ti-bearing minerals thus would make the melts gradually deplete in Sn, which is not favorable for late hydrothermal Sn mineralization (Linnen et al. 1995; Blevin 2004; Bhalla et al. 2005; Wang et al. 2017). Actually, because of the high oxygen fugacity, cassiterite will also crystallize earlier, leading to the melts being depleted in Sn. On the contrary, in the conditions of F-enriched and low f_{O2}, Sn is presented dominantly as an Sn^{2+} species (Linnen et al. 1996), the solubility of which is higher than the Sn^{4+} (Bhalla et al. 2005; Che et al. 2013). If no Sn-bearing mineral was fractioned from the melts, the Sn^{2+} would be gradually enriched in the residue melts and thus finally enter the magmatic-hydrothermal fluids, contributing to generate the ore-forming fluids (Wang et al. 2017).

Sr–Nd–Hf isotopic studies showed that the Sn-related and the W-related granites have some difference in source materials, of which more mantle materials were involved in the Sn-related granites while more crustal materials were involved in the W-related (Li et al. 2009; Liu et al. 2010a; Liu 2011; Chen et al. 2013; Su and Jiang 2017). This indicates that the redox conditions of the different magmas were probably originally controlled by the source materials.

5 Conclusion

1. LA-ICP-MS zircon U–Pb dating ($\sim$ 140 Ma for Sn-related granites, and $>$ 150 Ma for W-related granites) indicates that the Sn-related and W-related magmas were derived from two independent magmatic events rather than from cogenetic evolutionary series due to fractional crystallization.
2. Zircon Ce^{4+}/Ce^{3+} ratios indicate that the granites related to the Sn mineralization (Yanbei and Mikengshan) had lower oxygen fugacities than those related to the W mineralization (Tieshanlong, Qianlishan and Yaogangxian). This finding supports the effective indication of zircon for magmatic oxygen fugacity.

Acknowledgements We gratefully acknowledge Liyan Wu and Youwei Chen for field sampling, Yanwen Tang and Jun Yan for experiments, and Leiluo Xu and Wei Gao for data processing. This work was supported by the National Basic Research Program of China (973 Program) (Grants No. 2014CB440906), Innovation Team Program of Chinese Academy of Sciences (Overseas Famous Scholars Program) and "Light of West China" Program of Chinese Academy of Sciences.

References

Ballard JR, Palin MJ, Campbell IH (2002) Relative oxidation states of magmas inferred from Ce(IV)/Ce(III) in zircon: application to porphyry copper deposits of northern Chile. Contrib Mineral Petrol 144(3):347–364

Barth AP, Wooden JL (2010) Coupled elemental and isotopic analyses of polygenetic zircons from granitic rocks by ion microprobe, with implications for melt evolution and the sources of granitic magmas. Chem Geol 277(1–2):149–159

Belousova GW, O'Reilly SY, Fisher N (2002) Igneous zircon: trace element composition as an indicator of source rock type. Contrib Mineral Petrol 143(5):602–622

Bhalla P, Holtz F, Linnen RL, Behrens H (2005) Solubility of cassiterite in evolved granitic melts: effect of T, fO_2, and additional volatiles. Lithos 80(1–4):387–400

Blevin PL (2004) Redox and compositional parameters for interpreting the granitoid metallogeny of Eastern Australia: implications for gold–rich ore systems. Resour Geol 54(3):241–252

Blevin PL, Chappell BW, Allen CM (1996) Intrusive metallogenic provinces in eastern Australia based on granite source and composition. Trans R Soc Edinb Earth Sci 87:281–290

Burnham AD, Berry AJ (2012) An experimental study of trace element partitioning between zircon and melt as a function of oxygen fugacity. Geochim Cosmochim Acta 95:196–212

Burnham AD, Berry AJ (2014) The effect of oxygen fugacity, melt composition, temperature and pressure on the oxidation state of cerium in silicate melts. Chem Geol 366:52–60

Champion DC, Bultitude RJ (2013) The geochemical and Sr–Nd isotopic characteristics of Paleozoic fractionated S-types granites of north Queensland: implica-tions for S-type granite petrogenesis. Lithos 162–163:37–56

Che XD, Linnen RL, Wang RC, Aseri A, Thibault Y (2013) Tungsten solubility in evolved granitic melts: an evaluation of magmatic wolframite. Geochim Cosmochim Acta 106(4):84–98

Chen J (1993) Discontinuous evolution of the Shizhuyuan W, Mo, Bi and Sn skarn system in South China: fluid inclusion studies. J Nanjing Univ 993(3):439–447 **(in Chinese with English abstract)**

Chen J, Lu JJ, Chen WF, Wang RC, Ma DS, Zhu JC, Zhang WL, Ji JJ (2008) W-Sn-Nb-Ta-bearing granites in the Nanling Range and theirrelationship to metallogeny. Geol J Chin Univ 14:459–473 **(in Chinese with English abstract)**

Chen J, Wang RC, Zhu JC, Lu JJ, Ma DS (2013) Multiple-aged granitoids and related tungsten-tin mineralization in the Nanling Range, South China. Sci China Earth Sci 56:2045–2055

Chen YX, Li H, Sun WD, Irevor T, Tian XF, Hu YB, Yang WB, Chen C, Xu D (2016) Generation of LateMesozoic Qianlishan A2-type granite in Nanling Range, South China: implications for Shizhuyuan W-Sn mineralization and tectonic evolution. Lithos 266–267:435–452

Claiborne LL, Miller CF, Wooden JL (2010) Trace element composition of igneous zircon: a thermal and compositional record of the accumulation and evolution of a large silicic batholith, SpiritMountain, Nevada. Contrib Mineral Petrol 160(4):511–531

Dong SH (2012) Geochemistry of the Yaogangxian granite and implications for tungsten mineralization in southern Hunan Province. Institute of Geochemistry, Chinese Academy of Science, Beijing **(in Chinese)**

El-Bialy MZ, Ali KA (2013) Zircon trace element geochemical constraints on the evolution of the Ediacaran (600–614 Ma) post-collisional Dokhan volcanics and Younger granites of SE Sinai, NE Arabian-Nubian Shield. Chem Geol 360–361:54–73

Ferry JM, Watson EB (2007) New thermodynamic models and revised calibrations for the Ti-in-zircon and Zr-in-rutile thermometers. Contrib Mineral Petrol 154(4):429–437

Gan GL (1988) The characteristic of inclusions in minerals of the Huangsha vein-type tungsten deposit, Jiangxi. J Guilin Coll Geol 1988(2):35–41 **(in Chinese with English abstract)**

Hanchar JM, Westrenen W (2007) Rare earth element behavior in zircon-melt systems. Elements 3:37–42

Hayden LA, Watson EB (2007) Rutile saturation in hydrous siliceous melts and its bearing on Ti-thermometry of quartz and zircon. Earth Planet Sci Lett 258:561–568

Heaman LM, Bowins R, Crocket J (1990) The chemical composition of igneous zircon suites: implications for geochemical tracer studies. Geochim Cosmochim Acta 54:1597–1607

Hoskin PWO, Schaltegger U (2003) The composition of zircon and igneous and metamorphic petrogenesis. Rev Miner Geochem 53(1):27–62

Hu RZ, Zhou MF (2012) Multiple Mesozoic mineralization events in South China-an introduction to the thematic issue. Miner Depos 47(6):579–588

Hu RZ, Wei WF, Bi XW, Peng JT, Qi YQ, Wu LY, Chen YW (2012a) Molybdenite Re-Os and muscovite Ar-40/Ar-39 dating of the Xihuashan tungsten deposit, central Nanling district, South China. Lithos 150:111–118

Hu RZ, Bi XW, Jiang GH, Chen HW, Peng JT, Qi YQ, Wu LY, Wei WF (2012b) Mantle-derived noble gases in ore-forming fluids of the granite-related Yaogangxian tungsten deposit, Southeastern China. Miner Depos 47(6):623–632

Hu RZ, Mao JW, Hua RM, Fan WM (2015) Intra-continental mineralization of South China Craton. Science Press, Beijing, p 1 **(in Chinese)**

Hu RZ, Fu SL, Huang Y, Zhou MF, Fu SH, Zhao CH, Wang YJ, Bi XW, Xiao JF (2017a) The giant South China Mesozoic low-temperature metallogenic domain: review and a new geodynamic model. J Asian Earth Sci 137:9–34

Hu RZ, Chen WT, Xu DR, Zhou MF (2017b) Reviews and new metallogenic models of mineral deposits in South China: an introduction. J Asian Earth Sci 137:1–8

Hua RM, Chen PR, Zhang WL, Liu XD, Lu JJ, Lin JF, Yao JM, Qi HW, Zhang ZS, Gu SY (2003) Metallogenic systems related to Mesozoic and Cenozoic granitoids in South China. Sci China, Ser D Earth Sci 46(8):816–829

Huang F, Feng CY, Chen YC, Ying LJ, Chen ZH, Zeng ZL, Qu WJ (2011) Isotopic chronological study of the Huangsha-Tieshanlong Quartz Vein- type Tungsten deposit and timescale of molybdenum mineralization in Southern Jiangxi Province, China. Acta Geol Sin 85(6):1434–1447 (**English Edition**)

Li GL (2011) The evolution of Yanshanian granite and tungsten mineralization in Southern Jiangxi province and adjacent region. Nanjing University, Beijing **(in Chinese)**

Li HL, Bi XW, Tu GC, Hu RZ, Pen JT, Wu KX (2007) Mineral chemistry of biotite from Yanbei pluton: implication for Sn metallogeny. J Miner Pet 27(3):49–54 **(in Chinese with English abstract)**

Li XH, Li WX, Wang XC, Li QL, Liu Y, Tang GQ (2009) Role of mantle-derived magma in genesis of early Yanshanian granites in the Nanling Range, South China: in situ zircon Hf–O isotopic constraints. Sci China, Ser D Earth Sci 52:1262–1278

Li BL, Sun FY, Yu XF, Qian Y, Wang G, Yang YQ (2012) U–Pb dating and geochemistry of diorite in the eastern section from eastern Kunlun middle uplifted basement and granitic belt. Acta Petrol Sin 28(4):1163–1172 **(in Chinese with English abstract)**

Liang H (2017) Cretaceous porphyries associated with the porphyry Tin deposit in the Yanbei area, South China: petrogenesis and implications for mineralization. University of Chinese Academy of Sciences (Guangzhou Institute of Geochemistry, Chinese Academy of Sciences) **(in Chinese)**

Linnen RL, Pichavant M, Holtz F, Burgess SA (1995) The effect of Co_2 on the solubility, diffusion, and speciation of tin in haplogranitic melt at 850 C and 2 kbar. Geochim Cosmochim Acta 59(8):1579–1588

Linnen RL, Pichavant M, Holtz F (1996) The combined effects of f O2, and melt composition on SnO2, solubility and tin diffusivity in haplogranitic melts. Geochim Cosmochim Acta 60(24):4965–4976

Liu Y (2011) Crust-mantle interaction of Yanshanian granite magmatism in Qitianling-Daoxian region, Hunan. Doctoral Dissertation. Beijing: Chinese Academy of Geological Sciences **(in Chinese)**

Liu YS, Hu ZC, Gao S, Günther D, Xu J, Gao CG, Chen HH (2008) In situ analysis of major and trace elements of anhydrous minerals by LA-ICP-MS without applying an internal standard. Chem Geol 257(1–2):34–43

Liu Y, Li TD, Xiao QH, Geng SF, Wang XX, Chen BH (2010a) Magmatic mingling origin of adamellite: Zircon U-Pb dating and Hf isotopes evidence of microgranular microgranular dioritic enclaves and host rocks from Yangtianhu adamellite of Qitianling, South China. Geol China 37:1081–1091 **(in Chinese)**

Liu YS, Hu ZC, Zong KQ, Gao CG, Gao S, Xu J, Chen HH (2010b) Reappraisement and refinement of zircon U–Pb isotope and trace

element analyses by LA-ICP-MS. Chin Sci Bull 55(15):1535–1546

Mao JW, Pirajno F, Cook N (2011) Mesozoic metallogeny in East China and corresponding geodynamic settings—an introduction to the special issue. Ore Geol Rev 43(1):1–7

Mao JW, Cheng YB, Chen MH, Pirajno F (2013) Major types and time space distribution of Mesozoic ore deposits in South China and their geodynamic settings. Mine Depos 48:267–294

Mei YP, Li HQ, Wang DH, Lu YF, Yang HM, Xu JX, Zhang JJ (2007) Rock forming and ore-forming age of the Yanbei porphyry tin deposit in Jiangxi Province and their geological significance. Acta Geosci Sin 28(5):456–461 **(in Chinese with English abstract)**

Peng JT, Zhou MF, Hu RZ, Shen NP, Yuan SD, Bi XW, Du AD, Qu WJ (2006) Precise molybdenite Re–Os and mica Ar–Ar dating of the Mesozoic Yaogangxian tungsten deposit, central Nanling district, South China. Miner Depos 41(7):661–669

Pettke T, Audétat A, Schaltegger U, Heinrich CA (2005) Magmatic-to-hydrothermal crystallization in the W–Sn mineralized Mole granite (NSW, Australia): part II. Evolving zircon and thorite trace element chemistry. Chem Geol 220(3–4):191–213

Qiu JS, McInnes BIA, Jiang SY, Hu J (2005) Geochemistry of the Mikengshan pluton in Huichang County, Jiangxi Province and new recognition about its genetic type. Geochimica 34(1):20–32 **(in Chinese with English abstract)**

Qiu JS, Jiang SY, Hu J, McInnes BIA, Ling HF (2006) Isotopic dating of the Mikengshan tin ore-field in Huichang county, Jiangxi province, and its implications to metallogenesis. Acta Petrol Sin 22(10):2444–2450

Richards JP (2011) Magmatic to hydrothermal metal fluxes in convergent and collided margins. Ore Geol Rev 40(1):1–26

Richards JP (2013) Giant ore deposits formed by optimal alignments and combinations of geological processes. Nat Geosci 6:911–916

Shen WZ, Wang DZ, Xie YL, Liu CS (1995) Geochemical characteristics and material sources of the Qianlishan composite granite body, Hunan province. Acta Petrol Miner 3:193–202 **(in Chinese with English abstract)**

Smythe DJ, Brenan JM (2016) Magmatic oxygen fugacity estimated using zircon-melt partitioning of cerium. Earth Planet Sci Lett 453:260–266

Su HM, Jiang SY (2017) A comparison study of tungsten-bearing granite and related mineralization in the northern Jiangxi-southern Anhui provinces and southern Jiangxi Province in South China. Sci China Earth Sci (Earth Sci) 11:38–54

Sun SS, Mcdonough WF (1989) Chemical and isotopic systematics of oceanic basalts: implications for mantle composition and processes. Geol Soc Lond Spec Publ 42(1):313–345

Tong LH (2013) The petrogenesis and metallogenetic model of Qianlishan Tin–Tungsten bearing granite in Hunan. China University of Geosciences, Beijing

Trail D, Watson EB, Tailby ND (2011) The oxidation state of Hadeanmagmas and implications for early Earth's atmosphere. Nature 480(7375):79–82

Trail D, Watson EB, Tailby ND (2012) Ce and Eu anomalies in zircon as proxies for the oxidation state of magmas. Geochim Cosmochim Acta 97:70–87

Wang YL (2008) Tectonic–magma–mineralization of the W–Sn polymetallic ore concentration area in Southern Hunan Province. Chinese Academy of Geological Sciences **(in Chinese)**

Wang YL, Zhu XY, Peng QM, Fu QB, Li ST, Cheng XY (2014) Dark Inclusion in the Yaogangxian Granite, Hunan Province and its geochemical characteristics. Bull Mineral Petrol Geochem 33(3):299–308 **(in Chinese with English abstract)**

Wang RC, Xie L, Lu JJ, Zhu JC, Chen J (2017) Diversity of Mesozoic tin-bearing granites in the Nanling and adjacent regions, South China: distinctive mineralogical patterns. Sci China Earth Sci 60:1909–1919 **(in Chinese with English abstract)**

Watson EB, Harrison TM (2005) Zircon thermometer reveals minimum melting conditions on earliest Earth. Science 308(5723):841–844

Watson EB, Cherniak DJ, Hanchar JM (1997) The incorporation of Pb into zircon. Chem Geol 141:19–31

Watson EB, Wark DA, Thomas JB (2006) Crystallization thermometers for zircon and rutile. Contrib Mineral Petrol 151(4):413–433

Wei WF, Hu RZ, Bi XW, Peng JT, Su WC, Song SQ, Shi SH (2012) Infrared microthermometric and stable isotopic study of fluid inclusions in wolframite at the Xihuashan tungsten deposit, Jiangxi province, China. Miner Depos 47(6):589–605

Wu YB, Zheng YF (2004) Genesis mineralogy of zircon and its constraints on interpretation of U-Pb age. Chin Sci Bull 49(16):1589–1604 **(in Chinese with English abstract)**

Wu LY, Hu RZ, Peng JT, Bi XW, Jiang GH, Chen HW, Wang QY, Liu YY (2011) He and Ar isotopic compositions and genetic implications for the giant Shizhuyuan W–Sn–Bi–Mo deposit, Hunan Province, South China. Int Geol Rev 53(5–6):677–690

Yu ZF, Zhao HJ, Xu LG, Sun J, Liu Y, Zhang LC (2013) Characteristics of fluid inclusions and mineralization in Yanbei tin deposit in Jiangxi Province. Miner Depos 32(2):280–288 **(in Chinese with English abstract)**